The availability of filament ends modulates actin stochastic dynamics in live plant cells

Jiejie Li[a], Benjamin H. Staiger[a], Jessica L. Henty-Ridilla[a], Mohamad Abu-Abied[b], Einat Sadot[b], Laurent Blanchoin[c], and Christopher J. Staiger[a,d]

[a]Department of Biological Sciences, Purdue University, West Lafayette, IN 47907-2064; [b]Institute of Plant Sciences, Volcani Center, Bet-Dagan 50250, Israel; [c]Institut de Recherches en Technologie et Sciences pour le Vivant, Laboratoire de Physiologie Cellulaire et Végétale, Comissariat a l'Energie Atomique/Centre National de la Recherche Scientifique/Institute de la Recherche Agronomique/Université Joseph Fourier, F38054 Grenoble, France; [d]Bindley Bioscience Center, Purdue University, West Lafayette, IN 47907

ABSTRACT **A network of individual filaments that undergoes incessant remodeling through a process known as stochastic dynamics comprises the cortical actin cytoskeleton in plant epidermal cells. From images at high spatial and temporal resolution, it has been inferred that the regulation of filament barbed ends plays a central role in choreographing actin organization and turnover. How this occurs at a molecular level, whether different populations of ends exist in the array, and how individual filament behavior correlates with the overall architecture of the array are unknown. Here we develop an experimental system to modulate the levels of heterodimeric capping protein (CP) and examine the consequences for actin dynamics, architecture, and cell expansion. Significantly, we find that all phenotypes are the opposite for *CP*-overexpression (OX) cells compared with a previously characterized *cp*-knockdown line. Specifically, *CP* OX lines have fewer filament–filament annealing events, as well as reduced filament lengths and lifetimes. Further, *cp*-knockdown and OX lines demonstrate the existence of a subpopulation of filament ends sensitive to CP concentration. Finally, CP levels correlate with the biological process of axial cell expansion; for example, epidermal cells from hypocotyls with reduced CP are longer than wild-type cells, whereas *CP* OX lines have shorter cells. On the basis of these and other genetic studies in this model system, we hypothesize that filament length and lifetime positively correlate with the extent of axial cell expansion in dark-grown hypocotyls.**

Monitoring Editor
Thomas D. Pollard
Yale University

Received: Jul 10, 2013
Revised: Jan 31, 2014
Accepted: Feb 4, 2014

INTRODUCTION

The rapid turnover of actin filaments and remodeling of actin arrays are precisely regulated in eukaryotic cells. However, the molecular mechanisms underlying the construction of specific actin arrays in vivo remain under active investigation. Illuminating actin organization with molecular precision requires fast and high-resolution imaging systems. Variable-angle epifluorescence microscopy (VAEM) permits imaging at excellent signal to noise ratio of the cortical cytoplasm (Konopka and Bednarek, 2008) and has been used to generate analyses at high spatial and temporal resolution of individual actin filaments in living plant cells (Staiger *et al.*, 2009). Epidermal cells from *Arabidopsis thaliana* seedlings expressing the green fluorescent protein (GFP)–fABD2 reporter provide a facile model system to explore the mechanism of cytoskeletal turnover. In the dark-grown hypocotyl, which expands predominantly by cell elongation (Gendreau *et al.*, 1997), extent of bundling and abundance of actin filaments in the cortical array correlate with a gradient of axial cell expansion (Henty *et al.*, 2011; Li *et al.*, 2012). Specifically, cortical actin arrays exhibit decreased actin filament abundance and enhanced extent of bundling as one moves from fast-elongating cells at the apex of the hypocotyl toward the root, where cell expansion has ceased (Henty *et al.*, 2011; Li *et al.*, 2012). It is believed that actin arrays coordinate vesicle and organelle trafficking and thereby modulate delivery of cell wall materials and cellulose synthesis

This article was published online ahead of print in MBoC in Press (http://www.molbiolcell.org/cgi/doi/10.1091/mbc.E13-07-0378) on February 12, 2014.

Address correspondence to: Christopher J. Staiger (staiger@purdue.edu).

Abbreviations used: CP, capping protein; GFP, green fluorescence protein; MS, Murashige and Skoog; OX, overexpression; VAEM, variable angle epifluorescence microscopy.

machinery to plasma membrane (Crowell *et al.*, 2009; Gutierrez *et al.*, 2009; Szymanski and Cosgrove, 2009; Sampathkumar *et al.*, 2013).

Previous studies demonstrated that individual actin filament turnover in *Arabidopsis* epidermal cells occurs through a combination of rapid filament elongation at barbed ends and filament disassembly through prolific severing activity (Staiger *et al.*, 2009; Smertenko *et al.*, 2010; Henty *et al.*, 2011; Li *et al.*, 2012; Tóth *et al.*, 2012). Metrics have been developed to quantify key parameters of dynamic actin filaments, including elongation rate, severing frequency, filament–filament annealing, filament origin, and maximum filament length and lifetimes. The overall mechanism observed in living cells has been termed stochastic actin dynamics (Staiger *et al.*, 2009; Henty-Ridilla *et al.*, 2013). Actin filament turnover and generation of macromolecular structures are modulated by hundreds of actin-binding proteins (Pollard *et al.*, 2000; Pollard and Cooper, 2009). In plants, dozens of actin-binding proteins have been identified and their in vitro properties characterized extensively (Hussey *et al.*, 2006; Staiger *et al.*, 2009; Blanchoin *et al.*, 2010). Combining reverse-genetic approaches with quantitative image analysis of the cortical actin array provides a powerful platform to dissect the role of key actin-binding proteins in specific steps of actin turnover in vivo (Henty-Ridilla *et al.*, 2013). For example, high-spatiotemporal-resolution imaging of plant cells provided the first direct evidence for severing of actin filaments in vivo by ADF/cofilin family members and revealed the synergistic activity between ADF and AIP1 at the level of individual actin filament dynamics (Augustine *et al.*, 2011; Henty *et al.*, 2011).

The creation and availability of actin filament barbed ends have been suggested to play critical roles in the control of actin assembly in vivo. The ability to visualize the dynamic behavior of individual filament ends allows us to dissect the role of barbed-end regulation genetically. In *Arabidopsis* epidermal cells, new growing ends originate from three locations: de novo in the cytoplasm, from the side of existing filaments, or at the ends of preexisting fragments (Staiger *et al.*, 2009; Henty *et al.*, 2011; Li *et al.*, 2012). After initiation, actin filaments elongate from the putative barbed end at rates of ~2 μm/s (Staiger *et al.*, 2009; Smertenko *et al.*, 2010; Henty *et al.*, 2011; Li *et al.*, 2012; Tóth *et al.*, 2012). The opposite end, presumably the pointed end of a growing filament, is observed to shrink only occasionally and at rates of ~0.3 μm/s (Staiger *et al.*, 2009; Henty *et al.*, 2011). Filament extension can also be generated by filament–filament annealing, which allows for bursts of actin assembly (Smertenko *et al.*, 2010; Li *et al.*, 2012). Filament–filament annealing occurs infrequently—on the order of ~2% of available filament ends in wild-type cells (Li *et al.*, 2012). In addition, most newly created ends generated by severing activity fail to regrow, with only ~3% elongating after a break (Staiger *et al.*, 2009; Smertenko *et al.*, 2010; Li *et al.*, 2012). These data suggest that the majority of the barbed ends are capped at or soon after their creation and that capping factors dissociate slowly (Staiger *et al.*, 2009). Little is known, however, about the molecular mechanism(s) by which the dynamic behavior of actin filament barbed ends is regulated in plant cells.

To address these questions, we developed a system to experimentally modulate the behavior of actin filaments by altering the abundance of the ubiquitous barbed-end capping protein (CP) in live epidermal cells. CP is a heterodimer of structurally related α- and β-subunits (Cooper and Sept, 2008). In vitro, CP binds to filament barbed ends with high affinity, preventing addition and loss of monomers, and it inhibits filament–filament annealing (Cooper and Sept, 2008; Huang *et al.*, 2003, 2006). Moreover, its barbed end–capping activity is negatively regulated by phosphoinositide lipids (PPIs) in vitro (Schafer *et al.*, 1996; Kim *et al.*, 2007; Kuhn and Pollard, 2007). Beside PPIs, CP from *Arabidopsis* also binds to the signaling lipid phosphatidic acid (PA; Huang *et al.*, 2006; Pleskot *et al.*, 2012, 2013). It was suggested that the interaction between CP and PA occurs in vivo and leads to filament uncapping (Li *et al.*, 2012; Pleskot *et al.*, 2013). Genetic evidence shows that loss-of-function or null mutants for CP cause defects in the generation of specific actin-based structures in various organisms. In budding yeast, for example, actin cables and patch formation are perturbed (Amatruda *et al.*, 1990, 1992; Kim *et al.*, 2004), whereas in crawling cells the distribution between lamellipodial and filopodial actin at the leading edge is altered (Hug *et al.*, 1995; Rogers *et al.*, 2003; Mejillano *et al.*, 2004). It has been speculated that these defects are due to enhanced actin assembly on free barbed ends (Hug *et al.*, 1995; Hopmann *et al.*, 1996; Hopmann and Miller, 2003; Kim *et al.*, 2004; Kovar *et al.*, 2005). However, increasing CP level does not necessarily have the opposite effect on actin organization and developmental phenotype. The exception is budding yeast, in which overexpression of CP slightly inhibits actin polymerization from barbed ends and leads to loss of actin cables and abnormal cell morphogenesis (Amatruda *et al.*, 1992; Kim *et al.*, 2004). In fission yeast, mild CP overexpression specifically affects contractile ring assembly during cytokinesis; however, the actin patches and cables appear normal, whereas these structures are perturbed in a *cp*-knockout mutant (Kovar *et al.*, 2005). Finally, the number of free barbed ends decreases in *Dictyostelium* cells with enhanced CP expression, but the amount of filamentous actin and cell growth are similar to those in wild-type cells (Hug *et al.*, 1995). These data suggest that precise control of the availability of barbed ends by CP is essential to build diverse actin networks during various biological processes. However, the extent to which this mechanism is driven by interaction between CP and barbed ends differs between cell types and organisms.

In this study, we combine advanced live-cell imaging with quantitative image analyses to characterize the changes in dynamic behavior of filament ends caused by altering CP levels in *Arabidopsis* epidermal cells. Our data provide a broader and deeper understanding of how barbed-end regulation contributes to actin filament turnover and actin array dynamics. Significantly, enhancing and inhibiting actin dynamic turnover has opposite effects on axial cell expansion in plants.

RESULTS

Organ and cell expansions are influenced by CP levels

We showed previously that reducing CP levels resulted in excess elongation of hypocotyls and epidermal cells (Li *et al.*, 2012). Here we hypothesize that overexpressing CP will cause the opposite effect on organ growth and axial cell expansion. To test this prediction, we generated plants with enhanced *CP* expression levels by stable integration of both *CPA* and *CPB* under the control of the *CaMV-35S* promoter. A homozygous knockdown mutant, *cpb-1*, characterized in a previous study (Li *et al.*, 2012) was used as a control for phenotypic analyses. In 20 *CP*-overexpression (OX) lines examined, the transcript levels for *CPA* and *CPB* were considerably increased (unpublished data). Thus we selected three independent lines (*CP* OX1–3) with increased transcript levels for further experiments (Figure 1A). In the *cpb-1* mutant, *CP* transcript levels for both subunits were decreased approximately twofold compared with wild-type seedlings, which was consistent with previous results (Figure 1A; Li *et al.*, 2012). To further verify these results, we determined CP protein levels by semiquantitative immunoblotting. As shown in Figure 1C, protein levels for both CP α- and β-subunits

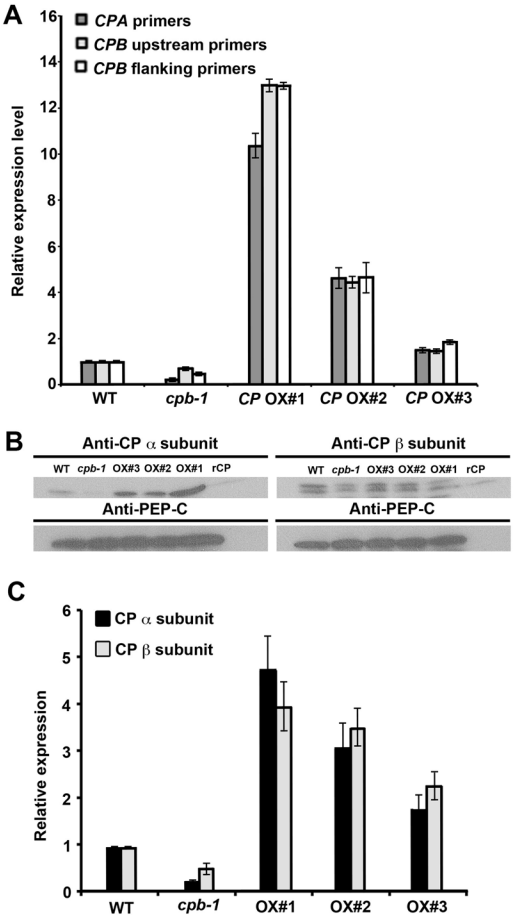

FIGURE 1: Transcript and protein levels for CPα and CPβ subunits are altered in *cpb-1* mutant and *CP*-overexpression lines. (A) qRT-PCR analysis of *CPA* and *CPB* transcript levels in 10-d-old, dark-grown seedlings from homozygous *cpb-1* mutant seedlings and three independent *CP*-overexpression lines (*CP* OX1–3). Col-0 wild-type (WT) seedlings were used as a control. (B) Western blot analysis of CP protein levels in WT, *cpb-1* mutant, and *CP* OX1–3 lines using anti-CPA and -CPB antibodies (Huang *et al.*, 2003). CP levels were considerably enhanced in three overexpression lines, whereas the *cpb-1* mutant had less CP protein expression than did WT. Blots are from one representative experiment. Recombinant CP (rCP) was included as a positive control and anti-PEPC antibody used as a loading control. (C) Protein levels in each genotype were measured quantitatively by densitometric analysis and plotted as fold induction compared with wild-type samples. Values are means ± SE from five biological replicates.

were increased up to fivefold in the *CP* OX lines. Moreover, the observation that individual lines had increasing amounts of transcript, with OX1 > OX2 > OX3, also held true at the protein level. In contrast, the *cpb-1*–knockdown line had ~20% of the CP α-subunit and ~50% of the β-subunit compared with wild type.

When grown under continuous dark conditions, *cpb-1* mutant seedlings exhibited longer hypocotyls than wild-type seedlings (Figure 2A; Li *et al.*, 2012). By contrast, all three *CP* OX lines showed strongly reduced hypocotyl lengths compared with wild-type and *cpb-1* mutant seedlings (Figure 2A). The differences between genotypes were significant throughout the developmental time period (Figure 2B). Of note, the extent of phenotypic defects in hypocotyl elongation correlated with CP level; specifically, the more transcript and protein present, the stronger was the growth-inhibition phenotype. To examine whether the differences in hypocotyl length resulted from defects in cell expansion, we measured epidermal cell length and width for all genotypes. The *cpb-1* mutant had significantly longer cells in all regions of dark-grown hypocotyls compared with wild-type hypocotyls (Figure 2C; Li *et al.*, 2012). By contrast, the *CP* OX lines showed severe reduction in cell length (Figure 2C). However, there were no differences in cell width between wild-type, *cpb-1*, and *CP* OX lines (Figure 2D).

Given that reduction of CP leads to shorter roots under light-grown conditions (Li *et al.*, 2012), we predicted that enhanced CP expression would affect root growth as well. As shown in Figure 3A, *CP* OX lines had significantly increased root length compared with wild type. Moreover, epidermal cells from the root elongation zone were significantly longer in *CP* OX lines than with wild-type cells and had the opposite phenotype to *cpb-1* mutant (Figure 3B). No significant difference in cell width was observed when wild-type, *cpb-1*, and *CP* OX lines were compared (Figure 3C). Under continuous dark-growth conditions, however, root lengths from either *cpb-1* mutant or *CP* OX lines did not have any significant difference when compared with wild type (unpublished data). One has to interpret such results from roots with a degree of caution, however, as organ length depends on both cell expansion and cell division, and the actin cytoskeleton is a target for proteasome-mediated destruction under dark-grown conditions (Dyachok *et al.*, 2011)

Collectively our results suggest that alteration of CP level affects organ and cell growth, specifically axial cell expansion. In addition, CP plays different roles or has varying levels of importance, depending on tissue type or developmental condition of the tissue.

CP levels affect cortical actin organization in epidermal cells

Biochemical studies demonstrate that *At* CP binds to actin filament barbed ends with high affinity and inhibits monomer addition and loss (Huang *et al.*, 2003, 2006). On the basis of these in vitro studies, we predict that the amount of functional CP in cells will inversely correlate with the availability of barbed ends for actin assembly, which thereby modulates F-actin levels. Specifically, we predict that an excess of CP will bind to all available barbed ends, regulating actin polymerization from the profilin-actin pool and thereby reducing overall filament levels (Huang *et al.*, 2006). To test this hypothesis, we observed the organization of cortical actin arrays in hypocotyl epidermal cells from wild-type, *cpb-1* mutant, and *CP* OX–line seedlings expressing the actin reporter gene *GFP-fABD2* (Sheahan *et al.*, 2004; Staiger *et al.*, 2009). In cells with reduced CP levels, actin arrays appeared to be denser than in wild-type cells (Figure 4, A and B; Li *et al.*, 2012), whereas the actin network in *CP* OX cells was sparser than in wild-type cells (Figure 4, C–E).

To compare these differences quantitatively, we measured the organization of actin arrays in epidermal cells with a set of tools described previously (Higaki *et al.*, 2010; Khurana *et al.*, 2010; Henty *et al.*, 2011; Li *et al.*, 2012). Two parameters, skewness and density, were applied to measure the extent of filament bundling and the percentage occupancy of actin filaments, respectively. As shown in Figure 4, F and G, and in a previous study (Li *et al.*, 2012), the percentage occupancy of actin filaments, or density of the actin array, in *cpb-1* mutant cells was significantly increased compared with wild-type cells; however, the actin arrays were moderately less bundled. In contrast, the abundance of actin filaments was reduced by 5–10% in *CP* OX cells relative to wild-type cells. The extent of bundling in *CP* OX1 cells was also slightly elevated; however, no significant differences in skewness values were detected between the other two *CP* OX lines and wild-type cells (Figure 4G).

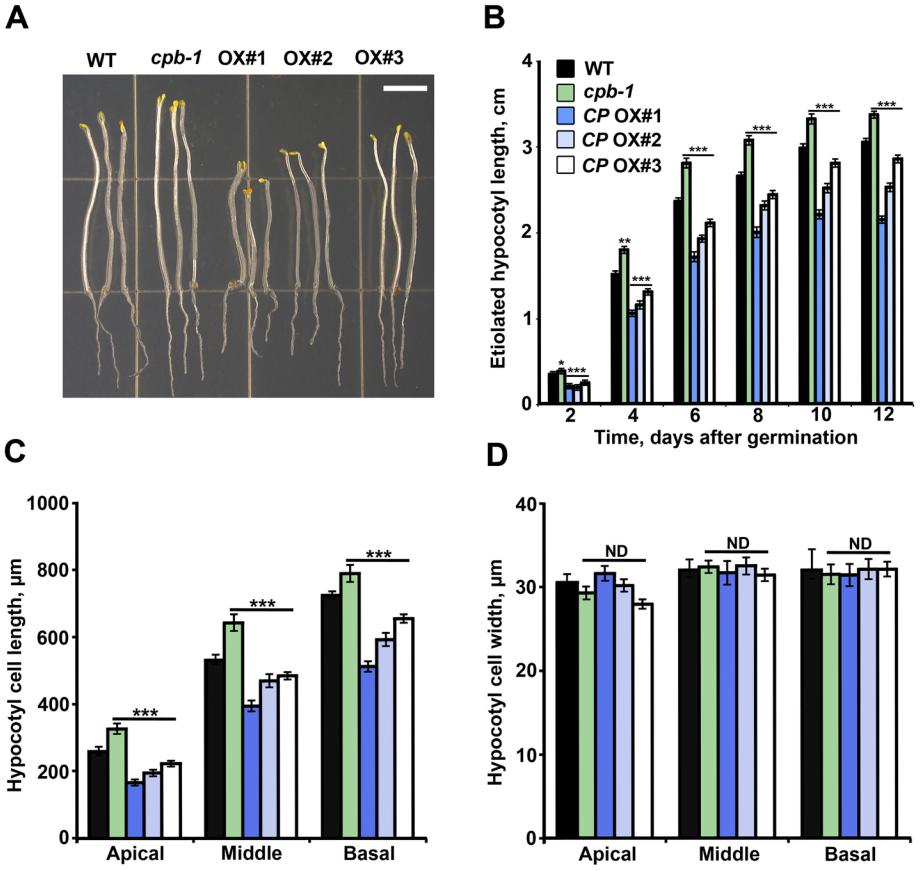

FIGURE 2: The extent of epidermal cell elongation correlates with CP levels in dark-grown hypocotyls. (A) Representative images of dark-grown hypocotyls from 5-d-old WT, *cpb-1*, and *CP* OX1–3. The hypocotyl–root junction from each seedling was aligned along a straight line for clarity. Bar, 0.5 cm. (B) Hypocotyl lengths were strongly reduced in *CP*-overexpression lines, whereas the *cpb-1* mutant had significantly longer hypocotyls than did WT (*$p < 0.05$; **$p < 0.01$; ***$p < 0.001$; *t* test). More than 50 seedlings/genotype were measured between 2 and 12 d after germination. Values are means ± SE. (C) Epidermal cell lengths were significantly shorter in *CP* OX1–3 than in WT cells. By contrast, cell lengths were significantly increased in *cpb-1* mutant, as shown previously (Li *et al.*, 2012). Measurements were performed on 5-d-old, dark-grown hypocotyls, and cells in the apical, middle, and basal one-third of the hypocotyl were binned into groups. Values represent means ± SE ($n > 300$ cells/genotype; ***$p < 0.001$; *t* test). (D) Measurements of cell width were performed on epidermal cells from 5-d-old, dark-grown hypocotyls, as described for C. No significant differences (ND) were observed among genotypes (*t* test).

Cortical actin array dynamics is altered by changes in CP levels

The cortical actin array in *Arabidopsis* hypocotyl epidermal cells undergoes incessant rearrangement and remodeling, with filament turnover occurring on time scales of tens of seconds (Figure 6A; Staiger *et al.*, 2009; Henty-Ridilla *et al.*, 2013). To investigate whether CP contributes to the overall dynamic behavior of actin networks, we monitored changes in actin arrays by time-lapse imaging of live epidermal cells in *cpb-1* mutant and *CP* OX lines. When compared with wild-type cells, the actin arrays in *cpb-1* mutant cells appeared more dynamic (Figure 6B), whereas the remodeling of actin filaments appeared less active in *CP* OX–line cells (Figure 6C). To quantify these changes in actin organization, we used a correlation coefficient analysis (Vidali *et al.*, 2010). This algorithm calculates the correlation coefficient for the intensity of each pixel at all possible temporal intervals. The extent of actin rearrangements over time was reflected by decay in the correlation coefficient as the temporal interval increased (Figure 6, D–G). The *cpb-1* mutant cells had a significantly faster decay than wild-type cells (Figure 6D), suggesting that the actin array rearrangements were more active due to reduction of CP. However, *CP* OX–line cells showed a slower decay in correlation coefficient values (Figure 6, E–G), which indicates that enhanced CP expression leads to decreased actin array dynamics. To confirm these results in another tissue, we applied the correlation coefficient analysis to time-lapse images of the cortical actin arrays in epidermal cells from the root elongation zone. The results were consistent with those in hypocotyl epidermal cells, with *CP* OX lines exhibiting less dynamic rearrangements and *cpb-1* having more dynamic arrays than wild-type root epidermal cells (Figure 5D). Collectively these data suggest that CP is involved in regulation of overall actin array dynamics.

In previous work, we demonstrated that reduced CP levels, or CP activity, led to altered organization of actin arrays in epidermal cells from the root elongation zone of light-grown seedlings (Li *et al.*, 2012; Pleskot *et al.*, 2013). To test whether overexpressing CP causes the opposite effect on actin organization in this organ, we quantified the changes in cortical actin architecture for all genotypes (Figure 5). Cells with enhanced CP levels showed significant decreases in actin filament abundance compared with wild-type cells (Figure 5, A and B). In *cpb-1* cells, the actin arrays were denser and less bundled, which is consistent with previous results (Figure 5, A–C; Li *et al.*, 2012). Moreover, the extent of actin filament bundling was modestly increased in *CP* OX1 cells (Figure 5C). Actin arrays in the other two *CP* OX lines showed no measurable differences in actin filament bundling compared with wild-type roots (Figure 5C). These results demonstrate that CP levels affect the density of actin filament arrays in plant epidermal cells. Reduced CP levels result in increased density of cortical actin arrays, whereas enhanced CP levels significantly decrease actin filament abundance.

The dynamic behavior of filament ends and actin filament turnover is affected by changes in CP levels

The dynamic properties of actin filament ends are precisely regulated in *Arabidopsis* epidermal cells (Henty-Ridilla *et al.*, 2013; Pleskot *et al.*, 2013). Previous observations suggest that a majority of the filament barbed ends are capped (Staiger *et al.*, 2009; Li *et al.*, 2012). However, uncapped barbed ends are available for fast elongation from a large pool of profilin–actin monomers, and some (~2%) ends can join together to elongate structures via filament–filament annealing (Staiger *et al.*, 2009; Smertenko *et al.*, 2010; Li *et al.*, 2012). Creating more uncapped ends in cells by reducing CP levels or inhibiting its activity leads to increased dynamic activities at filament ends, with significantly enhanced filament–filament annealing and an increased population of actin filaments originating from preexisting ends (Li *et al.*, 2012). Given that CP prevents barbed-end

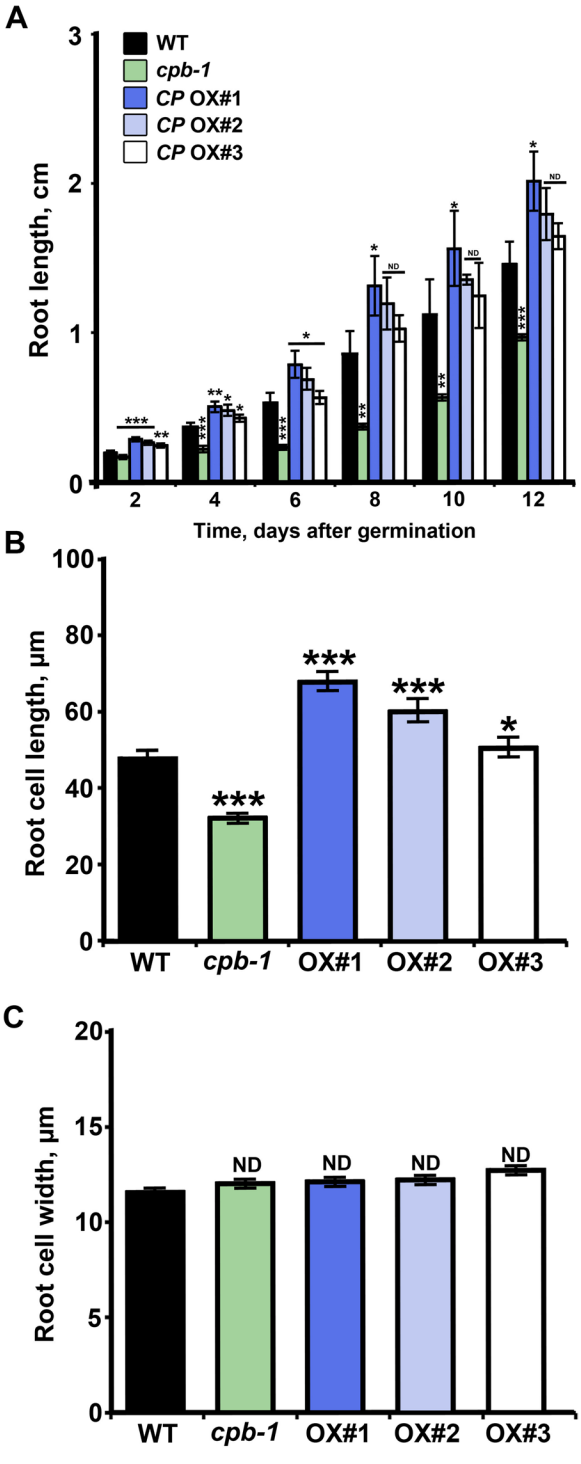

FIGURE 3: Overexpression of CP leads to longer root length. (A) Light-grown roots from the *cpb-1* mutant were significantly shorter than WT roots, as shown previously (Li *et al.*, 2012). By contrast, the root lengths in *CP* OX1 seedlings were significantly increased. Values are means ± SE from at least 50 seedlings/genotype measured 2–12 d after germination (*$p < 0.05$; **$p < 0.01$; ***$p < 0.001$; ND, no significant difference; *t* test). (B, C) Epidermal cells from the root elongation zone were significantly longer in *CP* OX1–3 seedlings, whereas cell lengths in *cpb-1* mutant were significantly reduced, when compared with WT (B). However, epidermal cell widths were not perturbed by altering CP levels in cells (C). Measurements were performed on 7-d-old, light-grown roots. Values are means ± SE ($n > 300$ cells/genotype; *$p < 0.05$; ***$p < 0.001$; ND, no significant difference; *t* test).

elongation of actin filaments and filament–filament annealing by blocking ends in vitro, we predict that increased CP levels could alter the properties of filament ends in cells. To address this, we monitored the dynamic behavior of filament ends by VAEM and quantified these behaviors in wild-type and *CP* OX line cells. The *cpb-1*–knockdown mutant was used as a control (Li *et al.*, 2012).

As shown in Table 1, CP overexpression prevents annealing of severed ends, with filament–filament annealing reduced to as little as 0% in *CP* OX1 when compared with wild-type cells (3.2%). In contrast, the frequency of filament–filament annealing in *cpb-1* cells increased more than fivefold compared with wild-type cells (Table 1). Further, the proportion of elongating filaments originating from different locations was altered by increasing CP levels, with a significant reduction in the filament population initiating from ends (21.8% in *CP* OX1 cells, 27.3% in wild-type cells; Table 1). By contrast, more filaments originated from the side of existing filaments or bundles in *CP*-overexpressing cells (~50%) compared with wild-type cells (40%; Table 1). In *cpb-1* cells, the percentage of filaments originating from ends was significantly increased by almost twofold compared with wild-type cells (Table 1) and is consistent with the previous study (Li *et al.*, 2012). Of note, there were still no significant differences in the frequency of filament regrowth from newly severed ends between any of the genotypes (Table 1; Li *et al.*, 2012).

In addition, *CP* OX cells had an effect on actin filament turnover. The filament lengths in *CP* OX lines decreased by as much as ~25% compared with wild type, whereas when the level of CP was reduced, filaments attained considerably longer maximum lengths, as shown previously (Li *et al.*, 2012). In addition, overexpressing CP leads to a significant reduction in filament lifetimes, as well as enhanced severing frequency, when compared with wild-type cells (Figure 7, A and C, Table 1, and Supplemental Videos S1 and S3). Reduced CP levels caused the opposite defects in these parameters when compared with overexpression lines, as shown previously (Table 1, Figure 7B, and Supplemental Video S2; Li *et al.*, 2012). These data confirm that CP is involved in the regulation of actin assembly by precise control of the availability of dynamic filament ends through overlapping mechanisms: CP inhibits annealing of severed fragments and terminates growth at a subset of the elongating barbed ends. Altering CP levels did not affect the regrowth frequency of newly severed ends, suggesting that CP is not required for this process.

Alteration of CP levels influences the proportion of filament ends with different elongation rates

In wild-type *Arabidopsis* epidermal cells, overall filament elongation rates averaged ~1.7 µm/s (Figures 7A and 8A). Changes in CP levels impaired this mean elongation rate (Table 1). In *cpb-1* mutant cells, the average actin filament elongation rate was moderately faster, as shown previously (Figure 8A; Li *et al.*, 2012). Overexpressing CP, however, shifted the population to slower rates (Figure 8A), with a significantly reduced average elongation rate of 1.46 µm/s in *CP* OX1 (Figure 8A and Table 1). In budding yeast, detailed analyses of the distribution of distinct populations of actin cables reveal different molecular mechanisms by which barbed-end elongation is coordinated (Chesarone-Cataldo *et al.*, 2011; Yu *et al.*, 2011). Specifically, actin cables with slow extension rates (<2 µm/s) are associated with different formins, whereas elongation rates >2 µm/s are due to filament translocations driven by the type V myosin, Myo2p (Chesarone-Cataldo *et al.*, 2011; Yu *et al.*, 2011).

We hypothesize that different populations of growing filament ends also exist in plant cells. To address this, we categorized the barbed-end elongation rates into three velocity populations and

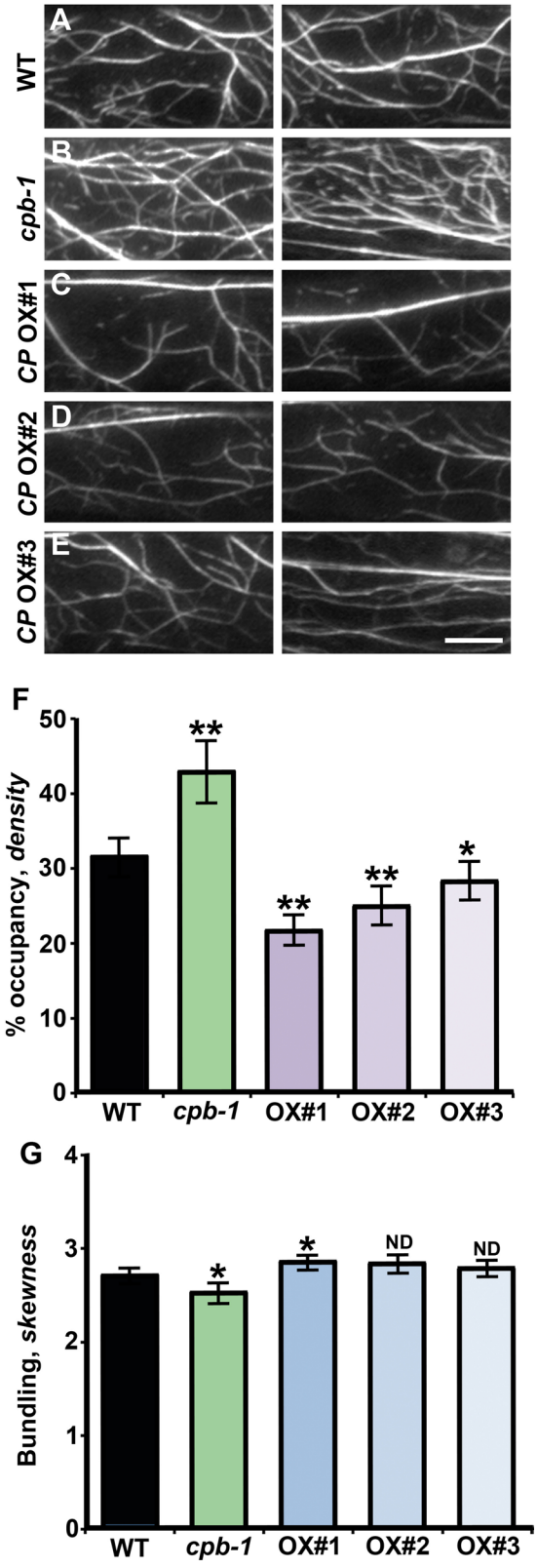

FIGURE 4: CP levels affect cortical actin organization in hypocotyl epidermal cells. (A–E) Representative images of epidermal cells expressing GFP-fABD2 from 5-d-old etiolated hypocotyls for WT (A), *cpb-1* (B), and *CP* OX1–3 lines (C–E). Images were collected by VAEM from the basal one-third of the hypocotyl. Bar, 10 μm. (F) Average filament density, or percentage of occupancy measurements, were determined on images collected from epidermal cells in the basal one-third of hypocotyls. The actin filament density was significantly decreased in *CP* OX1–3 lines. However, cortical actin arrays in the *cpb-1* mutant were denser than with respective wild-type controls, as shown previously (Li *et al.*, 2012). Values are means ± SE ($n \geq 500$ images from 10 hypocotyls/genotype; *$p < 0.05$; **$p < 0.01$; *t* test). (G) The extent of bundling (skewness) was measured on the same images used in F. The actin arrays in *cpb-1* mutant were modestly but significantly less bundled; in contrast, the extent of bundling was only slightly increased in *CP* OX1. Bundling analysis on the other two overexpression lines showed no significant difference from the respective wild-type controls (*$p < 0.05$; ND, no significant difference; *t* test).

calculated the percentage of each population, as described for budding yeast (Yu *et al.*, 2011). As shown in Figure 8B, the majority of filament barbed ends elongated at rates between 1 and 2 μm/s in wild-type cells. Only 4% grew at a rate <1 μm/s, and 28% elongated at rates >2 μm/s. In *cpb-1* mutant cells, the fast population of barbed ends increased by ~8% compared with wild-type cells (Figure 8B, gray bars). CP overexpression resulted in a reduced percentage of filaments with fast elongation rate; this population was lowered to ~10% in *CP* OX1 (Figure 8B, gray bars). Moreover, the population of barbed ends with slow rates increased to 18% in *CP* OX1 cells (Figure 8B, black bars). Among all of the genotypes, the proportion of filaments growing between 1 and 2 μm/s seemed to be unaffected (Figure 8B, white bars). These results suggested that, similar to budding yeast, there might be mechanistically distinct types of elongating barbed ends in *Arabidopsis* epidermal cells. We infer that CP prefers to associate with the fast-elongating barbed ends in cells. The precise interaction between CP and barbed ends is required for maintaining the normal distribution between populations of filament ends with different elongation rates.

DISCUSSION

To investigate the importance of filament barbed-end availability, we manipulated the levels of heterodimeric CP and evaluated the consequences for axial cell expansion, actin array architecture, and individual filament dynamics in living hypocotyl and root epidermal cells of *Arabidopsis*. Overexpression of CP led to shorter-than-normal hypocotyl epidermal cells, whereas CP knockdown resulted in increased axial cell expansion (Li *et al.*, 2012). CP levels also led to predictable changes in the density of actin filament arrays and overall actin array dynamics. More capped ends correlated with less-crowded cortical actin arrays and a reduction in overall actin dynamics. In contrast, cells with more free barbed ends had a greater density of filaments in the cortical array and increased dynamics (Li *et al.*, 2012). By examining directly the behavior of filament ends and individual actin filament turnover, we also found that CP overexpression reduces the number of filaments elongating at rates >2 μm/s and inhibits filament–filament annealing. Moreover, CP levels or activity contribute to actin filament turnover by modulating filament lengths and lifetimes. These data provide strong genetic and cytological evidence that regulation of filament end availability is a key cellular mechanism used to choreograph actin dynamics, organization of the cortical cytoskeletal array, and cell growth.

The barbed end of actin filaments is the favored site for actin polymerization in vitro (Pollard *et al.*, 2000). One can speculate that the extent of actin assembly is governed in part by the number and availability of barbed ends in cells. Based on its biochemical properties and cellular abundance, CP is considered to be a major filament end capper and regulator of actin assembly in vivo (Cooper and

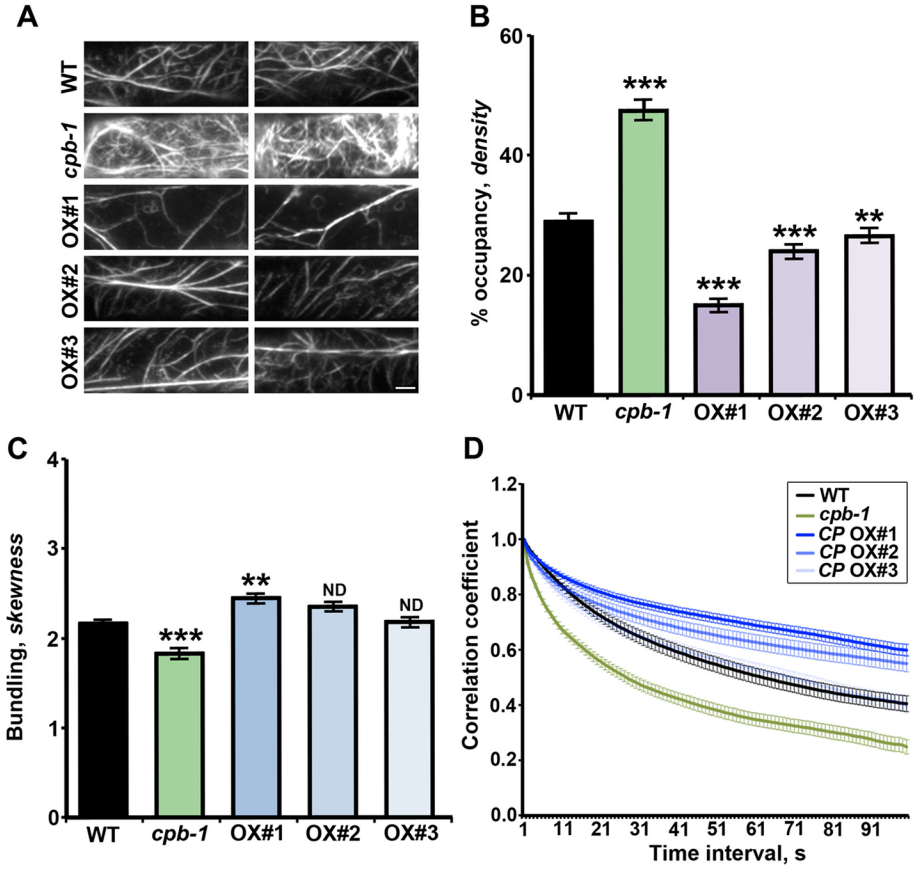

FIGURE 5: Cortical actin array organization and dynamics in epidermal cells from the root elongation zone are altered by changes in CP levels. (A) VAEM micrographs of the cortical actin array in epidermal cells from WT, *cpb-1*, and *CP* OX1–3 lines. Images were obtained from cells in the elongation zone of light-grown roots. Bar, 5 μm. (B) Average filament density, or percentage of occupancy measurements, were determined on images taken from epidermal cells in the root elongation zone of 7-d-old, light-grown seedlings. The percentage of occupancy (density) of actin filaments in the cortical array was significantly increased in *cpb-1* mutant, as shown previously (Li *et al.,* 2012; Pleskot *et al.*, 2013). By contrast, actin filament density in *CP* OX1–3 lines was significantly decreased compared with WT cells. (C) The extent of bundling (skewness) was measured on the same images used in A. The actin array in *CP* OX1 cells was slightly more bundled. By contrast, the extent of bundling in *cpb-1* mutant cells was modestly reduced when compared with WT cells. No significant differences from wild-type cells were shown in the other two overexpression lines by bundling analysis. Values in B and C are means ± SE ($n > 300$ images from 25 seedlings/genotype; $^{**}p < 0.01$; $^{***}p < 0.001$; ND, no significant difference; *t* test). (D) Cortical actin array dynamics was measured by correlation coefficient analyses on time-lapse VAEM series from WT, *cpb-1*, and three *CP* OX lines. The actin arrays in *cpb-1* mutant cells were significantly more dynamic. However, cells from *CP* OX lines had less dynamic actin arrays than did WT cells. Time-lapse series were recorded from epidermal cells in the root elongation zone of 7-d-old, light-grown seedlings. Values represent means ± SE ($n > 50$ time-lapse series/genotype; $p < 0.001$ for WT vs. *cpb-1* or *CP* OX1/2; $p > 0.05$ for WT vs. *CP* OX3; analysis of variance [ANOVA]).

Sept, 2008; Pleskot *et al.*, 2013). Genetic evidence from various organisms supports this assertion. In *Dictyostelium* and budding yeast, the number of free barbed ends inversely correlates with CP levels (Hug *et al.*, 1995; Kim *et al.*, 2004). Loss of CP results in an increase in the amount of filamentous actin, presumably due to more barbed ends being available for actin polymerization (Hug *et al.*, 1995; Hopmann *et al.*, 1996; Kim *et al.*, 2004; Kovar *et al.*, 2005). In contrast to other organisms, in which the majority of the total actin is present in polymer (Karpova *et al.*, 1995; Pollard *et al.*, 2000; Kim *et al.*, 2004), <5% of the G-actin pool is polymerized into filamentous actin in some plant cells (Gibbon *et al.*, 1999; Snowman *et al.*, 2002). Given that the total actin pool in *Arabidopsis* is estimated to be >50 μM, this is theoretically high enough to support robust actin assembly from free barbed ends (Staiger *et al.*, 2009; Henty-Ridilla *et al.*, 2013). Thus, to generate and maintain a relatively low density network, as found in the cortical array of hypocotyl epidermal cells, the precise regulation of CP to funnel subunits onto a limited number of free barbed ends becomes even more critical.

Here quantitative differences in the behavior of filament ends and the density of the cortical array caused by altered CP expression confirm this prediction. Cells in the *cpb-1* mutant had more dynamic ends, with a significantly increased population of elongating filaments that initiated from ends, and a fivefold increase in filament–filament annealing, as reported previously (Li *et al.*, 2012). Moreover, enhanced actin assembly onto ends of filaments correlated with denser actin arrays in the cortical cytoplasm of hypocotyl and root epidermal cells (Li *et al.*, 2012; Pleskot *et al.*, 2013). In contrast, increasing the abundance of CP caused the opposite effects on dynamic properties of filament ends and actin organization. For example, no annealing events were observed among the hundreds of ends we monitored in the *CP* OX1 line, and actin filament abundance was reduced significantly. This contrasts with results from other organisms, in which overexpression of CP does not necessarily lead to reduction in F-actin levels (Hug *et al.*, 1995; Kovar *et al.*, 2005), indicating that other mechanisms of actin assembly are required to maintain a constant ratio of G- to F-actin and can compensate for the effect of CP overexpression.

At the leading edge of migrating animal cells, the dynamics of lamellipodial actin is often measured by tracking GFP-actin speckles and extrapolating actin turnover rates from the average translocation rate of speckles in the network (Ponti *et al.*, 2004; Iwasa and Mullins, 2007). Depletion of CP impairs lamellipodial actin dynamics (Iwasa and Mullins, 2007), indicating that CP facilitates actin turnover in cells. Benefiting from the ability to visualize single-actin-filament dynamics in vivo (Staiger *et al.*, 2009; Henty *et al.*, 2011; Li *et al.*, 2012), we dissected the effects of CP on filament turnover in great detail. When compared with wild-type cells, elongating actin filaments in the *cpb-1* mutant extended for longer periods before suffering the first severing events (Figure 7B), which might result from less frequent capping events at the growing ends in the presence of reduced CP levels. By contrast, cessation of growth occurs much quicker in *CP* OX cells. We further quantified the turnover of single actin filaments by measuring key parameters such as maximum filament length and lifetime, as well as severing frequency. As shown in Table 1, cells with

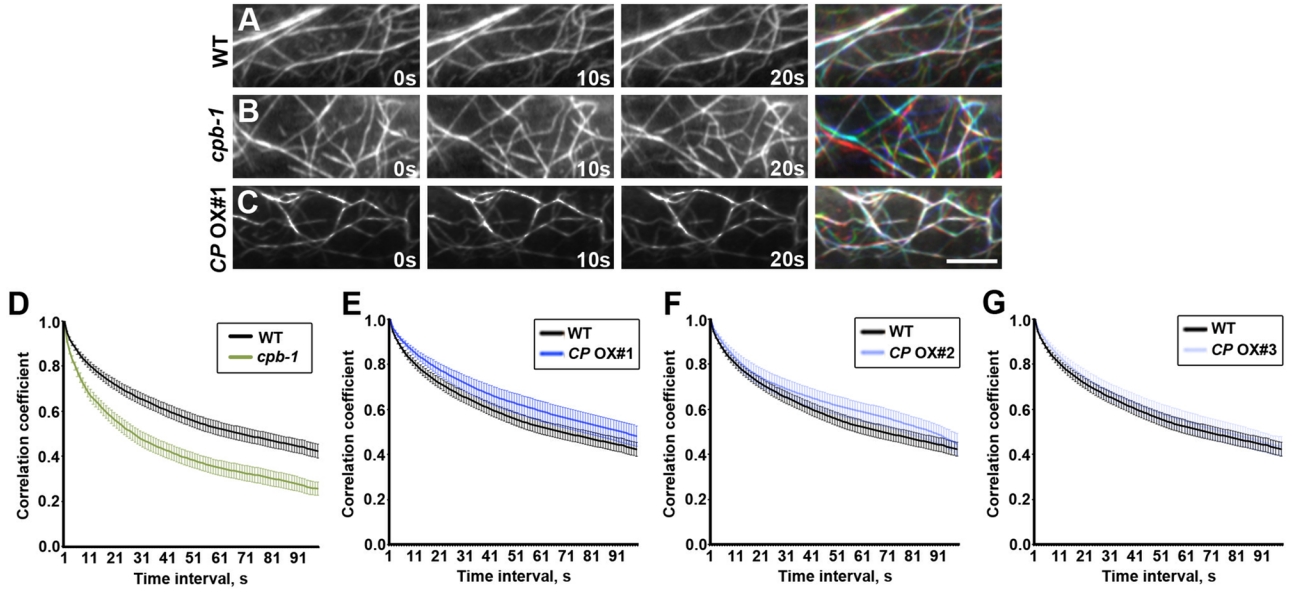

FIGURE 6: Cortical actin array dynamics is altered by changes in CP levels. (A–C) Representative images from time-lapse VAEM series taken at 10-s intervals from WT (A), *cpb-1* (B), and *CP* OX1 (C) hypocotyl epidermal cells. Images from three consecutive time points are colored red, green, and blue and merged in the right column. White indicates less-active actin structures during this time period. Bar, 10 μm. (D–G) Cortical actin array dynamics was measured by correlation coefficient analyses on time-lapse VAEM series from WT, *cpb-1* (D), and *CP* OX1–3 cells (E–G). The extent of actin rearrangement during a given time period was determined by decay in correlation as the temporal interval increased. The *cpb-1* mutant (D) showed much faster decay in the correlation coefficient values than did WT ($p < 0.0001$; ANOVA), whereas the *CP* OX1 line (E) showed slower decay than WT ($p < 0.0001$; ANOVA). The average correlation coefficient values at the indicated intervals were calculated from >40 time-lapse series taken from 10 hypocotyls for each genotype. Time-lapse series were recorded from epidermal cells in the basal one-third of 5-d-old, dark-grown hypocotyls. Error bars represent SE.

enhanced CP levels have significantly decreased filament lengths. Moreover, actin filaments in *CP* OX cells persist for a shorter period of time (Table 1 and Figure 7C). These behaviors of actin filaments are the opposite in *cpb-1* mutant cells (Table 1 and Figure 7B). Although severing frequency increases in *CP* OX plants, we do not believe that this reflects enhanced breakage activity. Because length is in the denominator of the calculation, altered filament length can influence the apparent frequency of events. In other words, reduction in maximum filament length in *CP* OX lines results in lower severing frequency, even though the number of breaks per unit time has not changed.

In addition to single-filament turnover, we explored how CP contributes to actin array dynamics on a macro scale. Using a correlation coefficient analysis that reports the extent of actin array

		WT	*cpb-1*	*CP* OX1	*CP* OX2	*CP* OX3
Elongation rate (μm/s)		1.71 ± 0.07	1.86 ± 0.06ND	1.46 ± 0.04**	1.54 ± 0.6*	1.58 ± 0.05*
Severing frequency (breaks/μm/s)		0.016 ± 0.001	0.012 ± 0.001***	0.024 ± 0.001***	0.023 ± 0.001***	0.017 ± 0.001ND
Maximum filament length (μm)		12.6 ± 0.6	15.7 ± 0.5***	9.5 ± 0.4***	9.5 ± 0.3***	11.8 ± 0.4ND
Maximum filament lifetime (s)		21.4 ± 0.9	26.0 ± 1.2**	18.3 ± 0.6**	20.2 ± 0.6ND	21.3 ± 0.6ND
Regrowth of severed ends (%)		3.2 ± 1.3	5.1 ± 1.7ND	2.2± 0.9ND	2.3 ± 1.2ND	3.3 ± 1.4ND
Annealing of severed ends (%)		3.2 ± 1.2	17.3 ± 4.0**	0.0 ± 0.0*	1.8 ± 0.9ND	2.2 ± 1.1ND
Filament origin (%/cell)	De novo	32.4 ± 1.8	23.7 ± 2.3	24.7 ± 2.4	28.3 ± 2.0	28.6 ± 2.0
	Ends	27.3 ± 2.2	42.0 ± 3.5††	21.8 ± 2.6††	24.7 ± 2.3†	25.9 ± 2.0ND
	Side	40.3 ± 2.1	34.3 ± 9.4	53.2 ± 2.9	46.7 ± 2.5	45.4 ± 2.7

Measurements taken from epidermal cells in the bottom one-third of 5-d-old hypocotyls from wild-type, *cpb-1*, and *CP* OX1–3 plants. Values are means ± SE, with $n > 50$ filaments from $n > 10$ epidermal cells and at least 10 hypocotyls/genotype. For filament origin: $n > 30$ cells from at least 10 hypocotyls/genotype.
ND, Not significantly different from wild-type control value by *t* test; $p > 0.05$.
*Significantly different from wild-type control value by *t* test; $p \leq 0.05$.
**Significantly different from wild-type control value by *t* test; $p \leq 0.01$.
***Significantly different from wild-type control value by *t* test; $p \leq 0.001$.
†Significantly different from wild-type control group value by ANOVA; $p < 0.05$
††Significantly different from wild-type control group value by ANOVA; $p < 0.0001$.

TABLE 1: Actin dynamics parameters for wild-type and *CP* mutant epidermal cells.

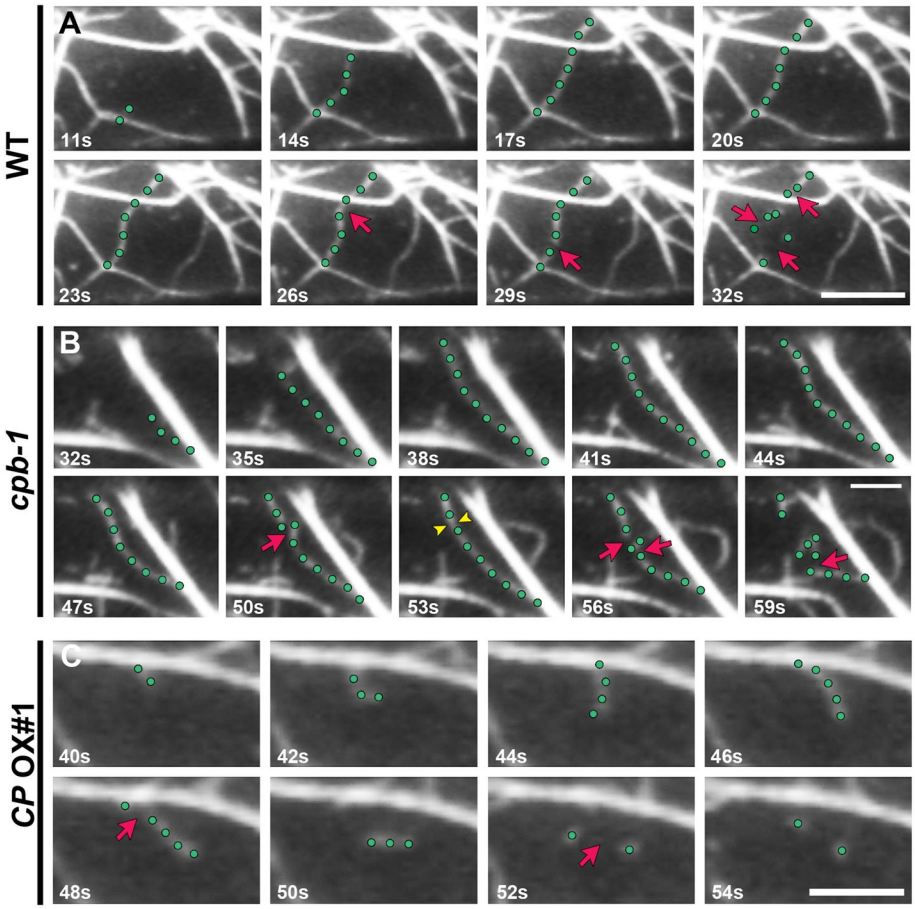

FIGURE 7: Changes in CP levels alter the dynamic behavior of single actin filaments in hypocotyl epidermal cells. (A) A representative actin filament from a WT epidermal cell (green dots) elongated rapidly and was subsequently dissembled by severing events (red arrows). Also see Supplemental Video S1. Bar, 10 µm. (B) A representative actin filament from a *cpb-1* mutant epidermal cell (green dots) elongated rapidly but persisted longer before severing events occurred (red arrows). Newly created ends sometimes joined together by filament–filament annealing (yellow arrowheads). Also see Supplemental Video S2. Bar, 5 µm. (C) A representative actin filament from a *CP* OX1–line epidermal cell (green dots) elongated slowly and was severed (red arrows) within 2 s after elongation ceased. Also see Supplemental Video S3. Bar, 5 µm. Images were collected by time-lapse VAEM from epidermal cells in the basal one-third of 5-d-old, dark-grown hypocotyls.

rearrangements over an entire temporal series (Vidali *et al.*, 2010), we showed that actin remodeling was much faster in cells with reduced CP levels than with wild-type cells. By contrast, the actin array in *CP* OX cells was less dynamic overall. It is noteworthy that the fast turnover of individual actin filaments does not necessarily lead to enhanced overall actin array rearrangements. The correlation coefficient analysis reveals the global changes in actin organization over time, which are influenced by a variety of events, including filament and bundle translocation, filament growth, and disassembly. By contrast, analysis of single-filament dynamics provides more detailed information about how the properties of a subpopulation of actin structures—individual actin filaments—are regulated. Thus one may not be able to directly correlate the changes in dynamic behaviors of individual actin filament with the causes of overall actin array rearrangements. Instead of actin filament turnover, the altered cortical array dynamics resulting from changes in CP levels may depend on the availability of dynamic ends, possibly via two potential mechanisms: 1) The availability of filament barbed ends is critical for regulating the extent of actin assembly in vivo, which can directly contribute to the cortical actin array dynamics. 2) Actin polymerization at barbed ends indirectly affects the abundance of filamentous actin that can be translocated in the cytoplasm.

It has been reported that CP regulates actin filament length by binding with high affinity and inhibiting monomer addition or loss from the barbed end in vitro (Cooper and Sept, 2008). Huang *et al.* (2003) showed that *Arabidopsis* CP causes a dose-dependent reduction in mean actin filament lengths in vitro. The regulation of filament length is suggested to be critical for cells to generate specific actin-based structures (Podolski and Steck, 1990; Pollard and Borisy, 2003; Pollard and Cooper, 2009). For example, at the leading edge of crawling cells, the lamellipodial actin is a dense actin meshwork composed of short actin filaments with high branching frequency (Pollard and Borisy, 2003). Computational simulation reveals that, during self-organization of a dendritic network, most filaments are capped before growing >0.5 µm (Schaus *et al.*, 2007). Several studies suggest that CP is required to maintain this dendritic meshwork, presumably by keeping filaments short (Hug *et al.*, 1995; Rogers *et al.*, 2003; Mejillano *et al.*, 2004; Iwasa and Mullins, 2007). Our data confirm the hypothesis that CP is necessary to regulate actin filament length in vivo. Specifically, actin filament length inversely correlates with the abundance of cellular CP. Elongating actin filaments in wild-type cells grow to ~13 µm before assembly ceases (Staiger *et al.*, 2009; Henty *et al.*, 2011; Li *et al.*, 2012). When the level of CP is reduced, filaments can attain considerably longer maximum lengths, as shown previously (Li *et al.*, 2012). By contrast, cells with enhanced CP expression had ~25% shorter filament lengths. Unlike mammalian cells (Mejillano *et al.*, 2004), long actin filaments in *cp* mutant do not lead to an increase in the extent of filament bundling in *Arabidopsis* epidermal cells (Li *et al.*, 2012), which indicates that the dendritic nucleation model may not explain the mechanism of cortical actin array organization in plant cells.

Individual actin filaments elongate rapidly in *Arabidopsis* epidermal cells, with an average rate of ~1.7 µm/s (Staiger *et al.*, 2009; Henty *et al.*, 2011; Li *et al.*, 2012), which means that ~630 monomers are assembled onto the barbed end per second (Staiger *et al.*, 2009). As pointed out earlier, a huge pool of assembly-competent actin monomers could drive this rapid elongation from free barbed ends (Henty-Ridilla *et al.*, 2013). In addition, processive elongation factors, such as formins, could enhance the growth rate even further. Formins are conserved proteins capable of both nucleating new filaments and facilitating processive subunit addition by persistent association with barbed ends (Goode and Eck, 2007). Only a few studies have demonstrated the latter property for formins from plants. A class II formin from the moss *Physcomitrella patens*, For2A, can

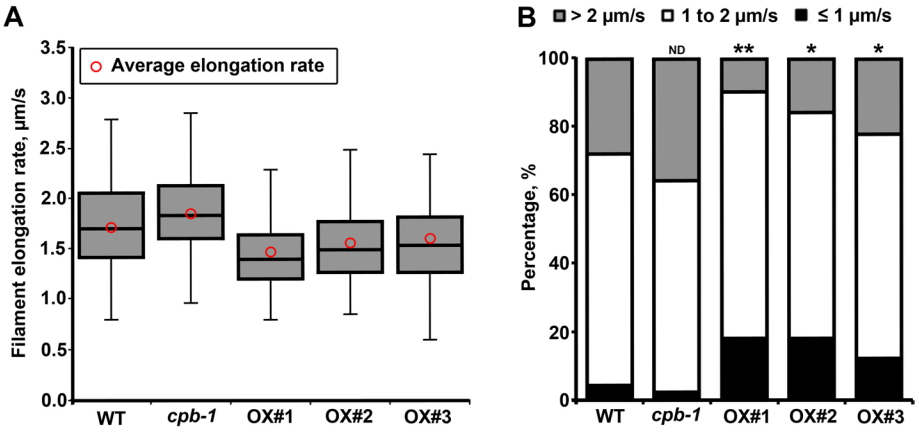

FIGURE 8: Proportion of filament ends with different elongation rates is altered in *cpb-1* mutant and *CP* OX lines. (A) Box plots show the elongation rates of filament ends measured in wild-type, *cpb-1* mutant, and *CP* OX–line cells. The box spans the first quartile to the third quartile. The line inside the box shows the median. The bars above and below the box show the minimum and maximum values. Red circles indicate the average filament elongation rates ($n \geq 100$ filaments/genotype). (B) Filament elongation rates from A were categorized into three velocity populations (Yu *et al.*, 2011): slow, <1 μm/s; intermediate, between 1 and 2 μm/s; and fast, >2 μm/s. Percentages of these populations were calculated. The majority of filaments in WT cells grew at intermediate rates. Cells in *cpb-1* mutant had a greater proportion of fast-growing ends than did WT cells, whereas the population of slow-growing ends significantly increased in *CP* OX1–3 cells ($n \geq 100$ filaments/genotype; $^*p < 0.05$; $^{**}p < 0.01$; *t* test).

promote the barbed-end elongation of actin filaments at rates that are 19 times faster than actin alone in vitro (Vidali *et al.*, 2009). Moreover, the For2A-associated filament ends elongate at 1.8 μm/s in moss cells (van Gisbergen *et al.*, 2012). *Arabidopsis* has >20 formin isoforms (Blanchoin and Staiger, 2010), but their characterization is incomplete. To gain further insights about the mechanisms of filament elongation in epidermal cells, we performed a more detailed analysis of barbed-end growth rates. Elongating filaments were categorized into three populations: fast (>2 μm/s), intermediate (between 2 and 1 μm/s), or slow (<1 μm/s) growing. We hypothesize that barbed ends elongating at different growth rates are either free barbed ends or associated with distinct formin isoforms. This hypothesis is supported by similar studies from yeast, where it has been shown that a subpopulation of actin cable elongation is regulated by specific formins (Chesarone-Cataldo *et al.*, 2011; Yu *et al.*, 2011). Combined with a state-of-art imaging system, similar reverse-genetics experiments could be applied to plant formin mutants (Rosero *et al.*, 2013), providing an unparalleled opportunity to dissect the function of plant formins in actin filament nucleation and assembly.

Altering the cellular abundance of CP in *Arabidopsis* influenced the proportion of actin filaments with different elongation rates. Only the populations of fast- and slow-growing filaments were affected by changes in CP level; the percentage of filaments growing at intermediate rates was similar between genotypes. These results suggest that CP terminates the growth of only the fast-growing (>2 μm/s) filament ends in cells. Moreover, we found that neither increasing nor decreasing CP expression impaired the regrowth frequency of newly severed ends, suggesting that there are multiple filament-end regulators in plants. Besides formins and CP, several classes of actin-binding proteins are known to control filament ends (Cooper and Schafer, 2000). Little is known about how the filament ends are controlled by these various end-binding proteins in cells and whether they are mechanistically different. Several studies demonstrate that actin-interacting protein1 (Aip1) interacts with actin filament barbed ends in budding yeast (Okreglak and Drubin, 2010; Michelot *et al.*, 2013). CP and Aip1 have overlapping functions but prefer different types of barbed ends (Michelot *et al.*, 2013). Loss of Aip1 in moss leads to a decrease in severing frequency, presumably due to reduced ADF/cofilin activity in *aip1* mutant (Augustine *et al.*, 2011). Collectively these data indicate the existence of distinct molecular mechanisms to regulate dynamic properties of filament ends, and these should be addressed in the future.

How actin array dynamics and organization regulate anisotropic cell expansion is a long-standing and unresolved issue in plant biology (Smith and Oppenheimer, 2005; Hussey *et al.*, 2006; Szymanski and Cosgrove, 2009). Studies on actin and actin-binding protein mutants demonstrate that disrupting actin array formation often results in cell expansion defects. However, the molecular mechanisms underlying these processes remain largely unknown. It has been suggested that the overall organization of cortical actin arrays does not necessarily correlate with cell expansion (Dyachok *et al.*, 2008; Henty *et al.*, 2011; Li *et al.*, 2012). For example, an *Arabidopsis adf4* mutant exhibits excessively bundled cortical actin arrays and enhanced axial cell expansion in dark-grown hypocotyls (Henty *et al.*, 2011). However, hypocotyl cells with reduced CP levels have denser and less-bundled actin arrays but still show enhanced cell elongation in this tissue (Li *et al.*, 2012). On the basis of the observation that maximum filament lengths and lifetimes are significantly increased in hypocotyl cells from both *adf4* and *cp* mutants (Henty *et al.*, 2011; Li *et al.*, 2012), we hypothesize that these properties are critical for actin-coordinating axial cell expansion, at least in dark-grown epidermal cells. Individual actin filaments could serve as tracks for positioning, retaining, and/or delivering Golgi-derived vesicles, which contain cell wall matrix polysaccharides or key enzymes such as the cellulose synthase complex (Gutierrez *et al.*, 2009; Sampathkumar *et al.*, 2013). Indeed, Ketelaar and coworkers showed that the Golgi apparatus made long excursions on actin filament bundles but much shorter translocations on dense actin meshworks (Akkerman *et al.*, 2011). Constructing arrays of filaments with increased lengths and lifetimes could provide longer and more stable tracks for enhanced vesicle delivery to the plasma membrane, where exocytosis occurs, which consequently would lead to enhanced axial cell expansion (*cpb-1*). If this model is correct, decreasing these two parameters of actin turnover should result in the opposite phenotype. Our new data confirm this hypothesis; CP overexpression caused a significant reduction in filament lengths and lifetimes. As a result, *CP* OX lines show decreased axial cell expansion of dark-grown hypocotyls. Although not tested directly, *act2act7* double mutants and latrunculin B treatments are predicted to result in shorter filament lengths and lifetimes, and these conditions also result in reduced axial cell expansion of hypocotyls (Baluska *et al.*, 2001; Kandasamy *et al.*, 2009; Sampathkumar *et al.*, 2013). In support of this model, it was demonstrated recently that chimeric myosins capable of transporting organelles at higher velocities than endogenous myosin XI correlate with enhanced cell expansion in *Arabidopsis*, whereas low-speed myosins have shorter cells (Tominaga *et al.*, 2013). However, additional studies on single-filament dynamics in other actin-binding

protein mutants with cell expansion defects will be required to further support this model.

MATERIALS AND METHODS

Plant material and growth conditions

All *A. thaliana* plants in this study were in the Columbia-0 (Col-0) background. The homozygous *cpb-1*–knockdown mutant (SALK_014783) was identified and characterized previously (Li *et al.*, 2012). The homozygous line was crossed to wild-type Col-0 expressing the GFP-fABD2 reporter (Sheahan *et al.*, 2004; Staiger *et al.*, 2009), and homozygotes were recovered from F2 populations (Li *et al.*, 2012). Seeds were surface sterilized and stratified at 4°C for 3 d on agar plates comprising half-strength Murashige and Skoog (MS) medium supplemented with 1% sucrose. For dark-grown hypocotyl length measurements, we grew stratified seeds in continuous darkness for 2–12 d after exposing the plates to light for 4 h. To analyze root growth, seedlings were grown vertically on 0.5× MS medium with 0% sucrose and 0.6% agar under long-day conditions (16 h light/8 h dark) at 21°C, as described previously (Dyachok *et al.*, 2011; Li *et al.*, 2012). To measure epidermal cell length and width, 5-d-old dark-grown hypocotyls were incubated in 5 µM FM4-64 dye (Invitrogen, Grand Island, NY) for 10 min. Every epidermal cell in a file along the long axis of the hypocotyl was imaged using a 10×/0.25 numerical aperture objective on a Nikon Microphot SA wide-field fluorescence microscope equipped with a charge-coupled device camera (ORCA-ER C4742-95; Hamamatsu Photonics, Middlesex, NJ); raw cell length and width values were binned into thirds based on the position along the hypocotyl. A double-blind experimental design was used for all phenotypic analyses. All image measurements were performed with ImageJ (National Institutes of Health, Bethesda, MD).

Generation of *CP*-overexpression lines

Transgenic *Arabidopsis* lines overexpressing heterodimeric CP were created by cotransforming Col-0 with two different binary vectors, each containing the full-length cDNA for *CPA* or *CPB* behind the *CaMV-35S* promoter. The full-length cDNAs for each subunit were amplified from the pET-23a-AB vector described previously (Huang *et al.*, 2003) with PCR and the following primers: CPA, 5′-GGGGTACCATGGCGGACGAAGAAGATGAG-3′ and 5′-CGGGATCCTCACAAATCCTTGAAAGTGTT-3′; and CPB, 5′-GGGGTACCATGGAGGCAGCTTTGGGACTT-3′ and 5′-CGGGATCCTCACAATGTGCAAACCATTTC-3′. The amplified products, with *Kpn*I and *Bam*HI sites introduced (underlined), were restriction digested, cloned into pBluescript II, and sequenced to verify their integrity. The coding sequences were removed from pBluescript-CPA or -CPB and subcloned into pART7 (Gleave, 1992) that was digested with *Kpn*I and *Bam*HI. The cassettes containing *35S* promoter, *CPA* or *CPB*, and the *ocs* terminator were removed by restriction with *Not*I and subcloned into the binary vector pART27 (Gleave, 1992). Alternatively, the expression cassette from pART7 was blunt ended and ligated into pCAMBIA1300 prepared with *Sma*I to generate binary vectors with hygromycin (hyg) resistance. All binary vectors were transformed into *Agrobacterium tumefaciens* strain GV3101. One plasmid each for CPA and CPB, with reciprocal selection markers (hyg and kan), was introduced into *Arabidopsis* plants by the floral-dip method (Zhang *et al.*, 2006). Transformants were selected in the T_2 generation on plates containing both antibiotics, and lines overexpressing CP identified by quantitative real-time (qRT)-PCR and semiquantitative immunoblots (see later description). Suitable T_3 lines were transformed with a binary vector, pMLBART:GFP-fABD2, and selected on Basta plates. All experiments were performed with T_4 lines.

RNA extraction and qRT-PCR

Ten-day-old, dark-grown seedlings were collected for total RNA isolation with TRIzol reagent (Invitrogen) according to the manufacturer's instructions. The isolated RNA was further treated with RQ1 DNase (Promega, Madison, WI). cDNA was synthesized using Moloney murine leukemia virus reverse transcriptase according to manufacturer's instructions (Invitrogen). To quantify gene expression, two-step qRT-PCR was performed using 2× SYBR Green master mix (Qiagen, Valencia, CA). Gene-specific primers for *CPA* (At3g05520) and *CPB* (At1g71790) used in this study were described previously (Li *et al.*, 2012). *GAPD* was used as an internal control to normalize gene expression across different samples. The fold change in the target gene, normalized to *GAPD* and relative to the gene expression in the control sample, was calculated as described (Khurana *et al.*, 2010). Three biological and technical replicates were performed per genotype.

Semiquantitative immunoblotting

Twenty-day-old, light-grown seedlings of wild-type, *cpb-1* mutant, and *CP* OX lines were used to estimate CP protein levels. About 0.2 g of whole-plant material was ground with liquid nitrogen into a fine powder and suspended with homogenization buffer containing 20 mM 4-(2-hydroxyethyl)-1-piperazineethanesulfonic acid/KOH, pH 7.2, 50 mM KOAc, 2 mM $Mg(OAc)_2$, 250 mM sorbitol, 1 mM EDTA, 1 mM ethylene glycol tetraacetic acid, 1 mM dithiothreitol, 1 mM phenylmethylsulfonyl fluoride, and 1% protease inhibitor cocktail (2 mM *o*-phenanthroline, 0.5 mg/ml leupeptin, 2 mg/ml aprotinin, 1 mg/ml pepstatin). This was followed by centrifugation at 4°C, 15,000 × *g* for 5 min, as described previously (Chaudhry *et al.*, 2007). Total protein concentration from supernatant was determined with the Bradford assay (Protein Assay; Bio-Rad, Hercules, CA) using bovine serum albumin as a standard. For each genotype, 50–75 µg of total protein was loaded on the same SDS–PAGE along with 5 ng of recombinant CP. Proteins separated by SDS–PAGE were transferred to nitrocellulose membranes and probed with anti-AtCPA and anti-AtCPB antibodies at a dilution of 1:2000, as described previously (Huang *et al.*, 2003). Phosphoenolpyruvate carboxylase (PEPC; Rockland Immunochemicals, Gilbertville, PA) was used as a loading control. The blots were incubated in horseradish peroxidase–coupled secondary antibody (Sigma-Aldrich, St. Louis, MO) at 1:100,000 dilution and developed with SuperSignal Pico West chemiluminescent substrate (Thermo Scientific, Rockford, IL) according to manufacturer's instructions. Densitometric analysis was performed for quantitative measurements of protein levels using ImageJ. Fold change in each CP subunit, normalized to PEPC and relative to protein levels in the control sample, was calculated. Five biological replicates were performed per genotype.

Quantitative analyses of the architecture of cortical actin arrays

The extent of actin filament bundling and percentage occupancy were measured using two parameters: skewness, based on the assumption that a population of actin filaments exhibits enhanced pixel intensities when bundled; and density, calculated as the percentage of occupancy of GFP-fABD2 signals in an image (Higaki *et al.*, 2010; Khurana *et al.*, 2010; Henty *et al.*, 2011; Li *et al.*, 2012). Epidermal cells in the basal one-third of 5-d-old, dark-grown hypocotyls or from the root elongation zone of 7-d-old, light-grown seedlings were

documented with a series of overlapping VAEM micrographs using fixed exposure time and gain settings for all the genotypes. Micrographs were analyzed in ImageJ using methods described previously (Higaki *et al.*, 2010; Henty *et al.*, 2011; Li *et al.*, 2012). All data analyses were performed as double-blind experiments.

Time-lapse imaging of actin filament dynamics in live cells

The cortical actin filament arrays in wild-type, *cpb-1* homozygous mutant, and *CP* OX–line seedlings were recorded by time-lapse VAEM, as described previously (Staiger *et al.*, 2009; Henty *et al.*, 2011; Li *et al.*, 2012). Epidermal cells from the basal one-third of 5-d-old, dark-grown hypocotyl, closest to the root, or from the root elongation zone of 7-d-old, light-grown seedlings were examined. All of the stochastic dynamic parameters were measured on time-lapse VAEM images from hypocotyl epidermal cells as described (Staiger *et al.*, 2009; Henty *et al.*, 2011; Li *et al.*, 2012). A double-blind experimental design was used to compare the stochastic dynamic parameters between genotypes. Time-lapse VAEM images for stochastic dynamics parameter measurements were also used for correlation coefficient analyses (Vidali *et al.*, 2010). Images were cropped to encompass a cell region containing GFP-fABD2 signal. Micrographs were analyzed in MATLAB using a method described previously (Vidali *et al.*, 2010).

ACKNOWLEDGMENTS

This study was funded through a grant (DE-FG02-09ER15526) from the Physical Biosciences Program of the Office of Basic Energy Sciences, U.S. Department of Energy, to C.J.S. A grant to E.S., M.A., and C.J.S. from the US–Israel Binational Agricultural Research and Development Fund (IS-4038-07) allowed the preparation of the *CP* OX constructs and transgenic lines. The TIRF microscopy facility was funded in part by the Bindley Bioscience Center at Purdue University. We are grateful to Hongbing Luo for excellent care and maintenance of plant materials.

REFERENCES

Akkerman M, Overdijk EJR, Schel JHN, Emons AMC, Ketelaar T (2011). Golgi body motility in the plant cell cortex correlates with actin cytoskeleton organization. Plant Cell Physiol 52, 1844–1855.

Amatruda JF, Cannon JF, Tatchell K, Hug C, Cooper JA (1990). Disruption of the actin cytoskeleton in yeast capping protein mutants. Nature 344, 352–354.

Amatruda JF, Gattermeir DJ, Karpova TS, Cooper JA (1992). Effects of null mutations and overexpression of capping protein on morphogenesis, actin distribution and polarized secretion in yeast. J Cell Biol 119, 1151–1162.

Augustine RC, Pattavina KA, Tüzel E, Vidali L, Bezanilla M (2011). Actin interacting protein1 and actin depolymerizing factor drive rapid actin dynamics in *Physcomitrella patens*. Plant Cell 23, 3696–3710.

Baluska F, Jasik J, Edelmann HG, Salajová T, Volkmann D (2001). Latrunculin B-induced plant dwarfism: plant cell elongation is F-actin dependent. Dev Biol 231, 113–124.

Blanchoin L, Boujemaa-Paterski R, Henty JL, Khurana P, Staiger CJ (2010). Actin dynamics in plant cells: a team effort from multiple proteins orchestrates this very fast-paced game. Curr Opin Plant Biol 13, 714–723.

Blanchoin L, Staiger CJ (2010). Plant formins: diverse isoforms and unique molecular mechanism. Biochim Biophys Acta 1803, 201–206.

Chaudhry F, Guérin C, von Witsch M, Blanchoin L, Staiger CJ (2007). Identification of *Arabidopsis* cyclase-associated protein 1 as the first nucleotide exchange factor for plant actin. Mol Biol Cell 18, 3002–3014.

Chesarone-Cataldo M, Guérin C, Yu JH, Wedlich-Soldner R, Blanchoin L, Goode BL (2011). The myosin passenger protein Smy1 controls actin cable structure and dynamics by acting as a formin damper. Dev Cell 21, 217–230.

Cooper JA, Schafer DA (2000). Control of actin assembly and disassembly at filament ends. Curr Opin Cell Biol 12, 97–103.

Cooper JA, Sept D (2008). New insights into mechanism and regulation of actin capping protein. Int Rev Cell Mol Biol 267, 183–206.

Crowell EF, Bischoff V, Desprez T, Rolland A, Stierhof Y-D, Schumacher K, Gonneau M, Höfte H, Vernhettes S (2009). Pausing of Golgi bodies on microtubules regulates secretion of cellulose synthase complexes in *Arabidopsis*. Plant Cell 21, 1141–1154.

Dyachok J, Shao M-R, Vaughn K, Bowling A, Facette M, Djakovic S, Clark L, Smith L (2008). Plasma membrane-associated SCAR complex subunits promote cortical F-actin accumulation and normal growth characteristics in *Arabidopsis* roots. Mol Plant 1, 990–1006.

Dyachok J, Zhu L, Liao F, He J, Huq E, Blancaflor EB (2011). SCAR mediates light-induced root elongation in *Arabidopsis* through photoreceptors and proteasomes. Plant Cell 23, 3610–3626.

Gendreau E, Traas J, Desnos T, Grandjean O, Caboche M, Höfte H (1997). Cellular basis of hypocotyl growth in *Arabidopsis thaliana*. Plant Physiol 114, 295–305.

Gibbon BC, Kovar DR, Staiger CJ (1999). Latrunculin B has different effects on pollen germination and tube growth. Plant Cell 11, 2349–2363.

Gleave AP (1992). A versatile binary vector system with T-DNA organizational structure conducive to efficient integration of cloned DNA into the plant genome. Plant Mol Biol 20, 1203–1207.

Goode BL, Eck MJ (2007). Mechanism and function of formins in the control of actin assembly. Annu Rev Biochem 76, 593–627.

Gutierrez R, Lindeboom JJ, Paredez AR, Emons AMC, Ehrhardt DW (2009). *Arabidopsis* cortical microtubules position cellulose synthase delivery to the plasma membrane and interact with cellulose synthase trafficking compartments. Nat Cell Biol 11, 797–806.

Henty JL, Bledsoe SW, Khurana P, Meagher RB, Day B, Blanchoin L, Staiger CJ (2011). *Arabidopsis* actin depolymerizing factor 4 modulates the stochastic dynamic behavior of actin filaments in the cortical array of epidermal cells. Plant Cell 23, 3711–3726.

Henty-Ridilla JL, Li J, Blanchoin L, Staiger CJ (2013). Actin dynamics in the cortical array of plant cells. Curr Opin Plant Biol 16, 678–687.

Higaki T, Kutsuna N, Sano T, Kondo N, Hasezawa S (2010). Quantification and cluster analysis of actin cytoskeletal structures in plant cells: role of actin bundling in stomatal movement during diurnal cycles in *Arabidopsis* guard cells. Plant J 61, 156–165.

Hopmann R, Cooper JA, Miller KG (1996). Actin organization, bristle morphology, and viability are affected by actin capping protein mutations in *Drosophila*. J Cell Biol 133, 1293–1305.

Hopmann R, Miller KG (2003). A balance of capping protein and profilin functions is required to regulate actin polymerization in *Drosophila* bristle. Mol Biol Cell 14, 118–128.

Huang S, Blanchoin L, Kovar DR, Staiger CJ (2003). *Arabidopsis* capping protein (AtCP) is a heterodimer that regulates assembly at the barbed ends of actin filaments. J Biol Chem 278, 44832–44842.

Huang S, Gao L, Blanchoin L, Staiger CJ (2006). Heterodimeric capping protein from *Arabidopsis* is regulated by phosphatidic acid. Mol Biol Cell 17, 1946–1958.

Hug C, Jay PY, Reddy I, McNally JG, Bridgman PC, Elson EL, Cooper JA (1995). Capping protein levels influence actin assembly and cell motility in *Dictyostelium*. Cell 81, 591–600.

Hussey PJ, Ketelaar T, Deeks MJ (2006). Control of the actin cytoskeleton in plant cell growth. Annu Rev Plant Biol 57, 109–125.

Iwasa JH, Mullins RD (2007). Spatial and temporal relationships between actin-filament nucleation, capping, and disassembly. Curr Biol 17, 395–406.

Kandasamy MK, McKinney EC, Meagher RB (2009). A single vegetative actin isovariant overexpressed under the control of multiple regulatory sequences is sufficient for normal *Arabidopsis* development. Plant Cell 21, 701–718.

Karpova TS, Tatchell K, Cooper JA (1995). Actin filaments in yeast are unstable in the absence of capping protein or fimbrin. J Cell Biol 131, 1483–1493.

Khurana P, Henty JL, Huang S, Staiger AM, Blanchoin L, Staiger CJ (2010). *Arabidopsis* VILLIN1 and VILLIN3 have overlapping and distinct activities in actin bundle formation and turnover. Plant Cell 22, 2727–2748.

Kim Y, McCully ME, Bhattacharya N, Butler B, Sept D, Cooper JA (2007). Structure/function analysis of the interaction of phosphatidylinositol 4,5-bisphosphate with actin-capping protein. J Biol Chem 282, 5871–5879.

Kim Y-W, Yamashita A, Wear MA, Maéda Y, Cooper JA (2004). Capping protein binding to actin in yeast: biochemical mechanism and physiological relevance. J Cell Biol 164, 567–580.

Konopka CA, Bednarek SY (2008). Variable-angle epifluorescence microscopy: a new way to look at protein dynamics in the plant cell cortex. Plant J 53, 186–196.

Kovar DR, Wu J-Q, Pollard TD (2005). Profilin-mediated competition between capping protein and formin Cdc12p during cytokinesis in fission yeast. Mol Biol Cell 16, 2313–2324.
Kuhn JR, Pollard TD (2007). Single molecule kinetic analysis of actin filament capping: polyphosphoinositides do not dissociate capping proteins. J Biol Chem 282, 28014–28024.
Li J, Henty-Ridilla JL, Huang S, Wang X, Blanchoin L, Staiger CJ (2012). Capping protein modulates the dynamic behavior of actin filaments in response to phosphatidic acid in *Arabidopsis*. Plant Cell 24, 3742–3754.
Mejillano MR, Kojima S, Applewhite DA, Gertler FB, Svitkina TM, Borisy GG (2004). Lamellipodial versus filopodial mode of the actin nanomachinery: pivotal role of the filament barbed end. Cell 118, 363–373.
Michelot A, Grassart A, Okreglak V, Costanz M, Boone C, Drubin DG (2013). Actin filament elongation in Arp2/3-derived networks is controlled by three distinct mechanisms. Dev Cell 24, 182–195.
Okreglak V, Drubin DG (2010). Loss of Aip1 reveals a role in maintaining the actin monomer pool and an in vivo oligomer assembly pathway. J Cell Biol 188, 769–777.
Pleskot R, Li J, Žárský V, Potocký M, Staiger CJ (2013). Regulation of cytoskeletal dynamics by phospholipase D and phosphatidic acid. Trends Plant Sci 18, 496–504.
Pleskot R, Pejchar P, Žárský V, Staiger CJ, Potocký M (2012). Structural insights into the inhibition of actin-capping protein by interactions with phosphatidic acid and phosphatidylinositol (4,5)-bisphosphate. PLoS Comput Biol 8, e1002765.
Podolski JL, Steck TL (1990). Length distribution of F-actin in *Dictyostelium discoideum*. J Biol Chem 265, 1312–1318.
Pollard TD, Blanchoin L, Mullins RD (2000). Molecular mechanisms controlling actin filament dynamics in nonmuscle cells. Annu Rev Biophys Biomol Struct 29, 545–576.
Pollard TD, Borisy GG (2003). Cellular motility driven by assembly and disassembly of actin filaments. Cell 112, 453–465.
Pollard TD, Cooper JA (2009). Actin, a central player in cell shape and movement. Science 27, 1208–1212.
Ponti A, Machacek M, Gupton SL, Waterman-Storer CM, Danuser G (2004). Two distinct actin networks drive the protrusion of migrating cells. Science 305, 1782–1786.
Rogers SL, Wiedemann U, Stuurman N, Vale RD (2003). Molecular requirements for actin-based lamella formation in *Drosophila* S2 cells. J Cell Biol 162, 1079–1088.
Rosero A, Žárský V, Cvrčková F (2013). AtFH1 formin mutation affects actin filament and microtubule dynamics in *Arabidopsis thaliana*. J Exp Bot 64, 585–597.
Sampathkumar A, Gutierrez R, McFarlane H, Bringmann M, Lindeboom J, Emons A-M, Samuels L, Ketelaar T, Ehrhardt D, Persson S (2013). Patterning and life-time of plasma membrane localized cellulose synthase is dependent on actin organization in *Arabidopsis* interphase cells. Plant Physiol 162, 675–688.
Schafer DA, Jennings PB, Cooper JA (1996). Dynamics of capping protein and actin assembly in vitro: uncapping barbed ends by polyphosphoinositides. J Cell Biol 135, 169–179.
Schaus TE, Taylor EW, Borisy GG (2007). Self-organization of actin filament orientation in the dendritic-nucleation/array-treadmilling model. Proc Natl Acad Sci USA 104, 7086–7091.
Sheahan MB, Staiger CJ, Rose RJ, McCurdy DW (2004). A green fluorescent protein fusion to actin-binding domain 2 of Arabidopsis fimbrin highlights new features of a dynamic actin cytoskeleton in live plant cells. Plant Physiol 136, 3968–3978.
Smertenko AP, Deeks MJ, Hussey PJ (2010). Strategies of actin reorganisation in plant cells. J Cell Sci 123, 3019–3028.
Smith LG, Oppenheimer DG (2005). Spatial control of cell expansion by the plant cytoskeleton. Annu Rev Cell Dev Biol 21, 271–295.
Snowman BN, Kovar DR, Shevchenko G, Franklin-Tong VE, Staiger CJ (2002). Signal-mediated depolymerization of actin in pollen during the self-incompatibility response. Plant Cell 14, 2613–2626.
Staiger CJ, Sheahan MB, Khurana P, Wang X, McCurdy DW, Blanchoin L (2009). Actin filament dynamics are dominated by rapid growth and severing activity in the *Arabidopsis* cortical array. J Cell Biol 184, 269–280.
Szymanski DB, Cosgrove DJ (2009). Dynamic coordination of cytoskeletal and cell wall systems during plant cell morphogenesis. Curr Biol 19, R800–R811.
Tominaga M, Kimura A, Yokota E, Haraguchi T, Shimmen T, Yamamoto K, Nakano A, Ito K (2013). Cytoplasmic streaming velocity as a plant size determinant. Dev Cell 27, 345–352.
Tóth R, Gerding-Reimers C, Deeks MJ, Menninger S, Gallegos RM, Tonaco IA, Hübel K, Hussey PJ, Waldmann H, Coupland G (2012). Prieurianin/endosidin 1 is an actin-stabilizing small molecule identified from a chemical genetic screen for circadian clock effectors in *Arabidopsis thaliana*. Plant J 71, 338–352.
van Gisbergen PA, Li M, Wu S-Z, Bezanilla M (2012). Class II formin targeting to the cell cortex by binding $PI(3,5)P_2$ is essential for polarized growth. J Cell Biol 198, 235–250.
Vidali L, Burkart GM, Augustine RC, Kerdavid E, Tüzel E, Bezanilla M (2010). Myosin XI is essential for tip growth in *Physcomitrella patens*. Plant Cell 22, 1868–1882.
Vidali L, van Gisbergen PAC, Guérin C, Franco P, Li M, Burkart GM, Augustine RC, Blanchoin L, Bezanilla M (2009). Rapid formin-mediated actin-filament elongation is essential for polarized plant cell growth. Proc Natl Acad Sci USA 106, 13341–13346.
Yu JH, Crevenna AH, Bettenbühl M, Freisinger T, Wedlich-Söldner R (2011). Cortical actin dynamics driven by formins and myosin V. J Cell Sci 124, 1533–1541.
Zhang X, Henriques R, Lin S-S, Niu Q-W, Chua N-H (2006). *Agrobacterium*-mediated transformation of *Arabidopsis thaliana* using the floral dip method. Nat Protoc 1, 641–646.